



Leveraging prior strain rates effect during stress relaxation of Sn–1.7Ag–0.7Cu lead-free alloys with microalloying of Te and Co for microelectronics applications

A. A. El-Daly¹ · K. M. Zohdy² · M. A. Abdo¹ · N. A. M. Eid¹

Received: 14 May 2019 / Accepted: 25 June 2019 / Published online: 1 July 2019
© Springer Science+Business Media, LLC, part of Springer Nature 2019

Abstract

Prior strain rate history during stress relaxation (SR) behavior is one of the fundamental issues adapting the design of solder joints. In this paper, the SR tests were performed on Sn–1.7Ag–0.7Cu (SAC177) solder with Te and Co addition at the elastic region. The SR of SAC177 solders occurred at high prior deformation history could induce unexpected relaxation resistance depending on the qualified proportions of Te and Co microalloying. The global strain rate $\dot{\epsilon}_p$ of three solders was found to follow the power-law with stress-sensitivity n of 5.8–7.6. The activation energies Q of 58.15–78.23 kJ mol⁻¹ were achieved from SR results at initial stress σ_0 of 10 MPa. An evolved SR model based on logarithmic single barrier model is intended in the present study to predict and confirms the SR mechanism. Microstructure assessment shows that the SR behaviors are controlled by pipe diffusion assisted with dislocation climb. According to the proposed relaxation model, the extent of SR and SR rate of SAC177 solder were found to be decreased markedly with increasing prior strain rate, Q value and Te/Co addition. Moreover, significant enrichment in the elastic compliance of SAC177 solders was noticed after Te/Co addition due to increasing the ductility, which has good predictions for electronics applications.

1 Introduction

Solders are a kind of metallic materials that can be used in all electronics industry since the growing of electronics era. The eutectic or near-eutectic Sn–Pb solder were used for assembling electronics owing to its high reliability, appropriate solderability, manufacturability and low pricing [1]. Because of the intrinsic toxicity of Pb-based solders, extensive attempts have been implicated to design innovative Sn-based lead-free solders for electronic interconnection. The Sn–Ag–Cu(SAC) alloy family is one of the highest promising alternative to Sn–Pb solders that could apply in flip-chip electronic interconnections, ball grid arrays (BGA) and other multiple electronic packages in modern electronic technology [2]. Recently, the low Ag-content SAC solders system has been developed by microalloying of metallic elements such as, Zn, Bi, Sb, Ni, nanoparticles, etc. [3, 4]. It

is recognized that the shrinking of volume fraction of large platelet Ag₃Sn phase in these low-Ag SAC solders could improve their mechanical properties and enrich their reliability [4–6]. For instance, Zn can refine Ag₃Sn IMC particles of SAC103 solders and formed the (Cu,Ag)₅Zn₈ IMC particles that enhance the yield strength (YS) with largest ductility [7, 8]. Bi particles addition to SAC157 solder leads to substantial increase in ultimate tensile strength (UTS), YS and Young's modulus, while the ductility was sustained at the SAC157 level [9].

Since the solder joints operate at elevated homologous temperatures ($T/T_m \approx 0.4–0.8$, T_m is the eutectic temperature), the microstructural instability and the variation in coefficients of thermal expansion (CTE) at the substrate are of great concern [10]. These severe process conditions could deteriorate the electrical connector, which intended to encounter the most performance requests at end of suitable life of components. Therefore, the annihilation of initial bonding force with time at substrate is one of the foremost topics in the design of solder joints. The annihilation of initial bonding force gives rise to an open circuit. For this reason, the SR test is a reliable method for assessment the contact force and its deformation mechanism [11]. Despite the

✉ A. A. El-Daly
dreldaly11@yahoo.com; dreldaly@zu.edu.eg

¹ Physics Department, Faculty of Science, Zagazig Univ, Zagazig, Egypt

² Higher Technological Institute, 10th of Ramadan City, Egypt

other aspects, such as alloy components, time, temperature, initial stress and grain size, the prior deformation history of strain rate on SR behavior is the vital aspect affecting the solder joints. For instance, the σ_0 levels imposed before SR in eutectic Sn–40Pb, Sn–4Ag, and Sn–2.5Ag–0.8Cu–0.5Sb at 23 °C were found to depend on the prior strain rates, i.e. high SR could result in higher cyclic deformation histories of strain rates [12]. However, since it is hard to design solder joints with definite amount of normal stress at the contact interface, the designed force must be improved to verify the end-of-suitable life force. For this reason, the prior deformation history could enhance the designed force to verify the end-of-suitable life force. Until this work, no systematic study has been reported on the effect of prior deformation history on stress relaxation behavior of low-Ag SAC177 solder. In this study, the influence of prior strain rate on SR behavior of SAC177 solder has been investigated at different processing conditions of temperatures. At the same time, microalloying of Te and Co elements were added to enhance the microstructure and modifying the design of SAC177 solder joints. The effects of Te and Co microalloying on the growth rate of Ag_3Sn and Cu_6Sn_5 IMCs and SR behavior have been discussed in this paper. SR tests were carried out to evaluate the controlling deformation mechanisms at different temperature conditions for SAC177 solders.

2 Experimental procedures

The low-Ag content SAC177, SAC177-0.2Te and SAC177-0.5Co alloys with the chemical compositions of Sn–1.7Ag–0.7Cu, Sn–1.7Ag–0.7Cu–0.2Te and Sn–1.7Ag–0.7Cu–0.5Co (wt%) were used for the study. The alloys were prepared from metal ingots of Sn (99.9%), Ag (99.999%), Cu, Co and Te (99.99%). The metal ingots were melted at 800 °C for ~1 h in a quartz tube under a KCl+LiCl (1.3:1) atmosphere in an induction furnace. The ingots melts were mechanically stirred to verify master alloy dissolution. The ingots were cast into a steel mold and left to cool at cooling rate of 6–8 °C/s, so as to construct microstructures typically create in small solder joints in electronic industries. In order to attain the surface quality demanded for scanning electron microscope (SEM) and EDS assessments, the samples were polished and etched with a solution of 3% HCl, 2% and HNO_3 in 95% ethyl alcohol for a few seconds. The prepared specimens were analyzed by XRD analysis to identify the precipitated phases in the solidified alloys. Then, tensile tests were done to measure the stress–strain and stress–time relations using computerized tensile testing system described previously [13]. A number of shaped rods for each of three alloys, having nominal gage diameters of 1.2×10^{-3} m with a gage length of 4×10^{-2} m, were prepared for tensile tests. Stress–strain tests were carried out first for a

small time to achieve the initial stress of 10 MPa at the elastic region. The tensile tests were performed at prior strain rates of $6.6 \times 10^{-5} - 3.5 \times 10^{-3} \text{ s}^{-1}$ and temperature range of 25–110 °C. And then, SR tests were performed immediately after each tensile test. The created imposed strain for each sample corresponding to the desired initial stress was then held constant to permit the initial stress of 10 MPa to relax for a sufficient relaxation time t_{SR} of 5000 s. However, the SR test was repeated three times for the entire alloy samples.

3 Results and discussion

3.1 Solidification microstructure of SAC177 based-alloys

To identify the primary phases in the solders, the as-cast microstructures are examined by XRD. As shown in Fig. 1, the Sn, Ag_3Sn and Cu_6Sn_5 phases are existed in SAC177, SAC177-0.2Te and SAC177-0.5Co alloy samples. It is also notable that Te- and Co-microalloying are effectively suppressed the diffraction peak intensity of Sn phase. This indicates that the crystallinity of three phases is refined with Te- and Co-microalloying. However, the affinity of Te into Sn to leads to formation of SnTe IMC particles in SAC177-0.2Te solder, while the high affinity of Co into Cu leads to formation of $(\text{Cu}, \text{Co})_6\text{Sn}_5$ IMC precipitates in the SAC177-0.5Co solder. Based on the XRD results of Fig. 1, our current understanding of modification by Te/Co additions to SAC177 solder alloy can be advanced. As shown in Fig. 2a, the as-solidified SAC177 alloy involves a fully eutectic structure of Ag_3Sn needles and Cu_6Sn_5 IMCs with

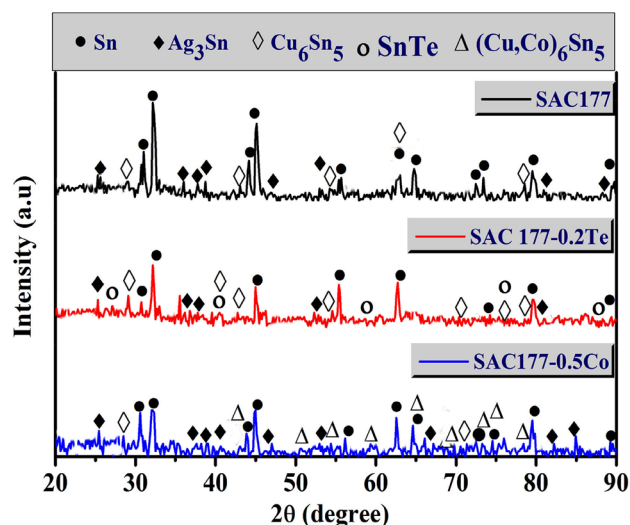
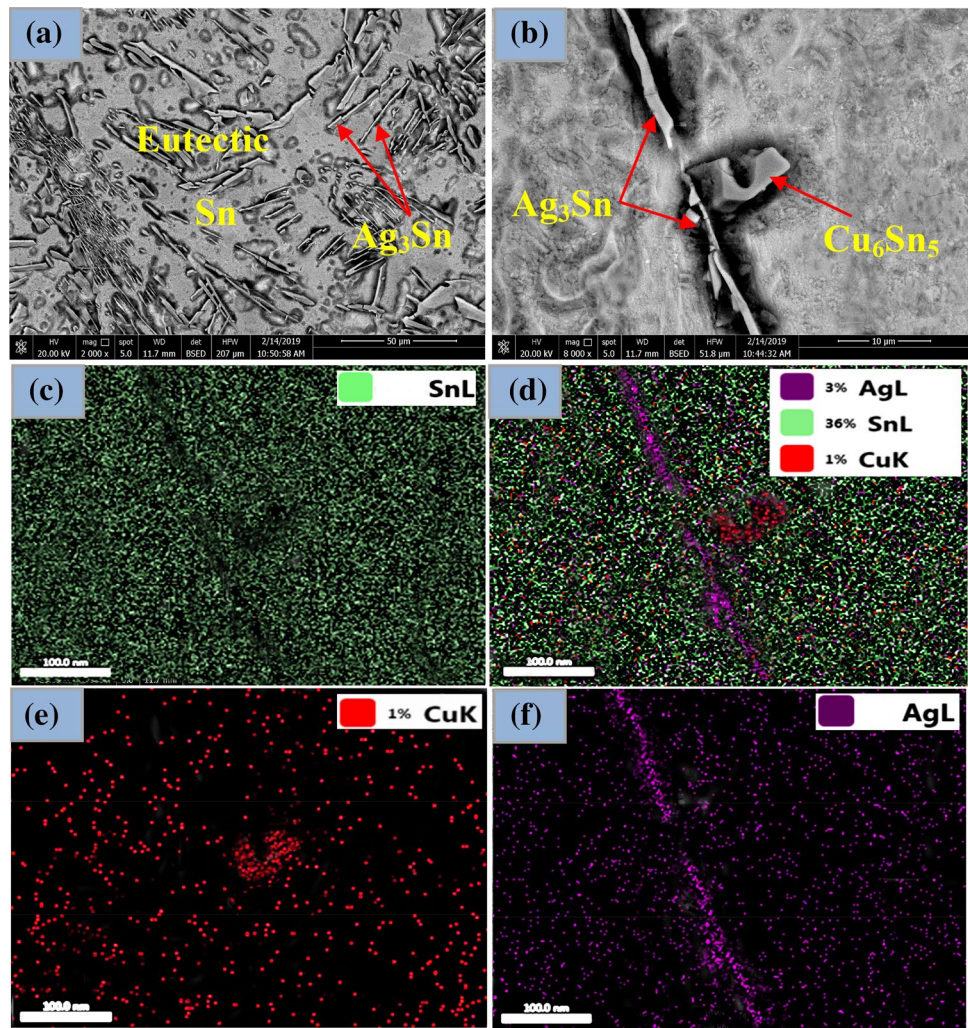


Fig. 1 XRD profiles of as-solidified SAC177, SAC177-0.2Te and SAC177-0.5Co alloys

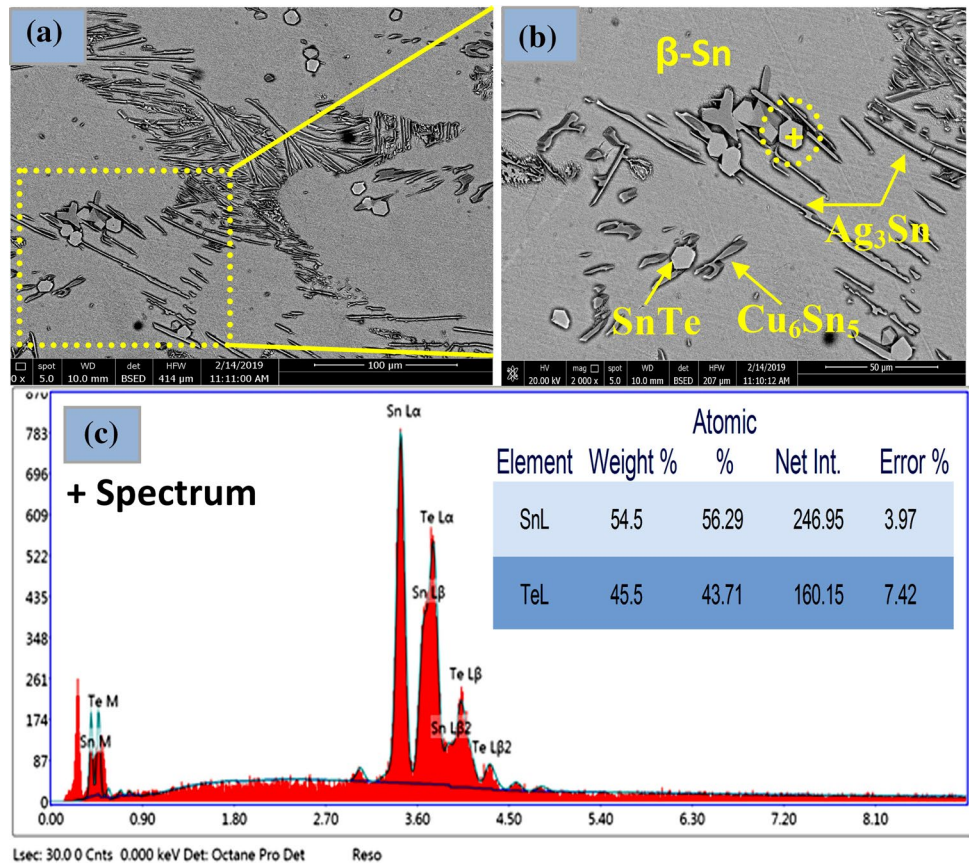
Fig. 2 Low and high magnification FE-SEM image of SAC177 solder and their corresponding EPMA elemental mappings of Sn, Ag and Cu, showing the microstructure of Cu_6Sn_5 and Ag_3Sn IMCs



haphazard distribution inside the β -Sn matrix. The average size of needle-like Ag_3Sn is approximately 7–30 μm , while for irregularly shaped Cu_6Sn_5 IMCs is about 4–7 μm . The dual-phase mixture is consistent with earlier work of SAC alloys [14]. The SEM-EPMA elemental map of SAC alloy microstructure in Fig. 2b–f shows that the starting microelectronic joint solder involves Sn, Cu and Ag. The microstructure of SAC177 is basically composed of Ag_3Sn and Cu_6Sn_5 phases inside β -Sn matrix. As a result, both the Cu_6Sn_5 and Ag_3Sn are at equilibrium in molten SAC177 alloy before nucleating the β -Sn phase. Compared with the basic SAC177 solder, the change in composition of IMC particles is detected with Te-microalloying as seen in Fig. 3a; Firstly, minor Te-microalloying (~ 0.2 wt%) can introduce new hexagonal SnTe particles (with an average size of ≤ 10 μm) within the eutectic and dendritic regions during the solidification process. Since the grain size of SnTe particles lies in the range of superplastic alloy materials, it will not induce micro-cracks. Therefore, these new IMC particles could be one of the causes that enhance the

SR resistance of SAC177-0.2Te solder. Secondly, the growth of primary β -Sn grains with the appropriate volume fraction of fine eutectic Cu_6Sn_5 and Ag_3Sn particles could promote the mechanical property of SAC177-0.2Te solder. Figure 3b, c estimates detailed views of FE-SEM micrograph and corresponding EDS analysis of SnTe IMC particles. However, the effective refinement of Cu_6Sn_5 and Ag_3Sn IMC particles contributed by minor amount of Te can be ascribed to its higher affinity. The higher affinity of Te to Sn atoms could reduce the activity of Sn, which reduces the driving force for Cu_6Sn_5 and Ag_3Sn IMC formation. Besides, SnTe particles can assist as an extra nucleation sites to promote the solidification process and retard the growth of IMCs. With Co addition, microstructure of SAC177 solder is significantly changed. Figure 4a shows the morphology progress of SAC177-0.5Co alloy. Clearly, 0.5wt% addition of Co into SAC177 solder leads to significant change in Ag_3Sn morphology from coarse needle-like (Fig. 2a) into small volume fraction of fine needle-shaped (Fig. 4a). The presence of fine IMC particles can positively affect the mechanical

Fig. 3 Low and high magnification FE-SEM image of SAC177-0.2Te alloy and corresponding EDS analysis of SnTe IMC particles



reliability of solder when this alloy solder applied on novel green microelectronic devices. However, the small Cu_6Sn_5 particles were found to be regularly distributed at the $\beta\text{-Sn}$ phase. As well, the dissolved Co and Cu elements are reacted with $\beta\text{-Sn}$ phase to form an excessive amount of long strip-shaped $(\text{Cu}, \text{Co})_6\text{Sn}_5$ IMC particles in solder matrix. As seen in Fig. 4b–g, the mapping of elements identified by EPMA shows the color mapping of Ag, Cu, Co and Sn elements. The $\beta\text{-Sn}$ -matrix plays the utmost detection for fine particles (violet-green-pink-red) spread softly over the view sample. It seems that the content of Sn was minor only at areas attendant with $(\text{Cu}, \text{Co})_6\text{Sn}_5$ and Ag_3Sn IMCs.

3.2 Strength and ductility

Drop impact reliability of solder joints has become one of vital topic for enhancing inventive portable electronics. To empathize this issue, a typical stress–strain tests for three SAC177, SAC177-0.2Te and SAC177-0.5Co alloys were conducted at strain rate of $5.8 \times 10^{-4} \text{ s}^{-1}$ and $T = 25^\circ \text{C}$. The results were presented in Fig. 5 and the yield stress YS, ultimate tensile stress UTS and elongation are summarized in the corresponding histogram. It is noted that the tensile behaviors of three alloys reflect the attendance of large plateau rejoins thanks to the relative equilibrium

of dynamic recovery with work hardening processes during deformation. However, the Te and Co microalloying is markedly enriched the drop impact reliability of SAC177 alloy. The additions of Te and Co are slightly increased YS and UTS of SAC177 solder, whereas the ductility is significantly increased due to refine the microstructure along with the grew of fine SnTe and Co_3Sn IMCs. The highest YS (28.0 MPa) and UTS (29.92 MPa) as well as elongation of 50.41% were observed for Co-containing solder. The Te and Co microalloying acknowledge the deformation to be “spread out” over the whole phases as well. The high stress and strain values of Co-containing solder could result in greater elastic compliance than that of SAC177 solder for innovative green microelectronic industry.

3.3 Stress relaxation dependence of prior strain rate

Figure 6a–c shows the SR behavior of three solders at different prior strain rates in terms of the decrease in yielding stress versus relaxation time. In all testing conditions, the amount of initial stress σ_0 was held constant at 10 MPa in the elastic region (lower than the YS point) at $T = 25^\circ \text{C}$. For better comparison of results, the SR responses are superimposed to explicate the influence of prior strain rates. As

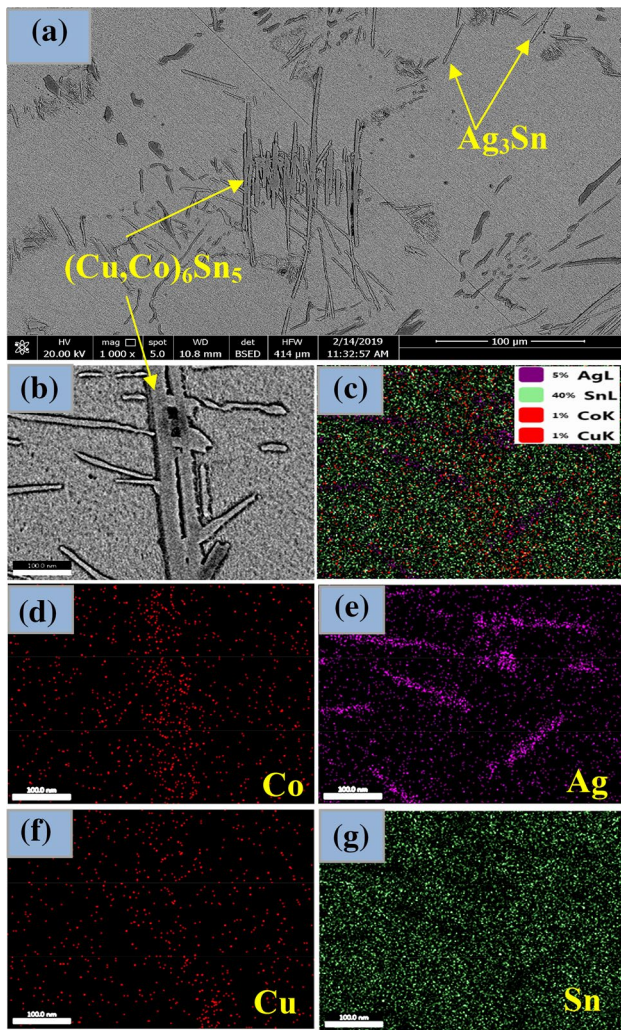


Fig. 4 FE-SEM image of SAC177-0.5Co alloy and corresponding EDS analysis of $(\text{Cu,Co})_6\text{Sn}_5$ IMC particles

noticed from the curves, the rate of stress relaxation is accelerated in the primary stage of relaxation at initial time of 1000–1500 s, followed by a slight rate decrease at extended times up to 5000 s. The drastic drop of SR is detected at ~ 2.36 MPa with prior strain rate of $6.6 \times 10^{-5} \text{ s}^{-1}$ for plain SAC177 solder, indicating the highest amount of relaxation $\Delta\sigma(t)$ [$\Delta\sigma = \sigma_0 - \sigma(t)$] and SR rate $\dot{\sigma}$ [$\dot{\sigma} = d(\Delta\sigma/d \ln(t))$] among all solders, as shown in Table 1. The slowing down of SR may develop as a result of hardening following the plastic deformation and the lessening in mobile dislocation density [15]. Although the entire SR curves in Fig. 6 show comparable trends, the final relaxed stress in three solders after 5000 s shows different SR behavior, depending on the initial imposed strain ϵ_0 or strain rate and alloy composition. For instance, at time of 5000 s, the total $\Delta\sigma$ is about 4.37, 4.02, 3.76 MPa, respectively, for SAC177, SAC177-0.2Te and SAC177-0.5Co solder samples at strain rate of $3.5 \times 10^{-3} \text{ s}^{-1}$, as seen in Table 1. The low SR rate $\dot{\sigma}$ for Te- and Co-containing solders is largely ascribed to dislocation interaction with SnTe and Co_3Sn IMCs that playing significant role in adapting deformation behavior despite the traditional dislocation–dislocation intersection. The dislocation loops accumulated nearby the IMC particles could generate internal stresses in the solder matrix, which leads to oppose the dislocation motion and hence could develop the strain hardening ability of Te- and Co-containing solders. However, the improvement in ϵ_0 values with prior strain rate during SR tests was the best for Co microalloying, as shown in Fig. 6d. Even so, the higher ϵ_0 values of 0.002–0.013 observed at all prior strain rates for three alloys confirm that plasticity has occurred below the YS point. The occurrence of plasticity could ascribe to the high fraction of β -Sn grain boundaries and fine IMCs that acting as main sources of dislocations. Remarkably, the more plasticity is detected with SAC177-0.5Co solder, followed by SAC177-0.2Te and SAC177

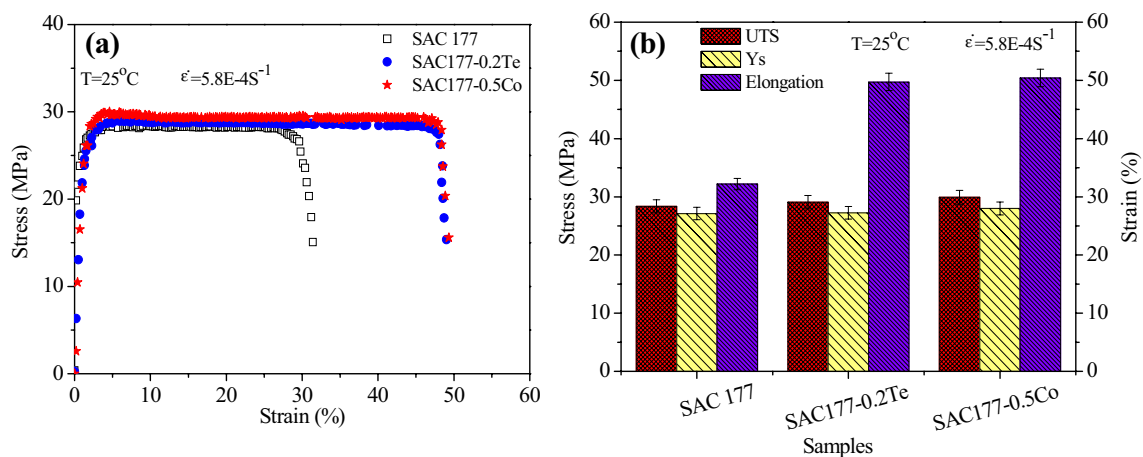


Fig. 5 Tensile stress–strain curves of SAC177, SAC177-0.2Te and SAC177-0.5Co alloys and corresponding histogram of yield stress YS, ultimate tensile stress UTS and elongation

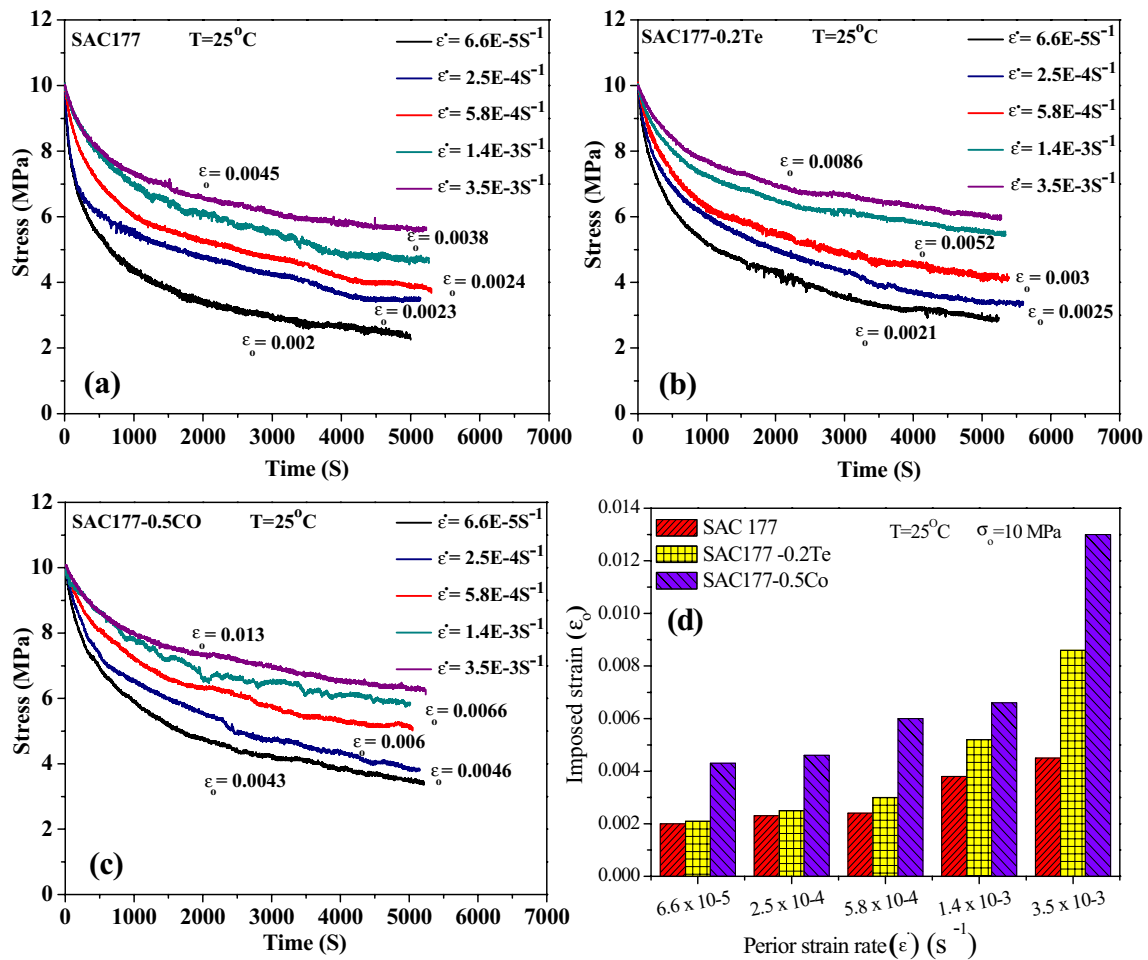


Fig. 6 Experimental stress relaxation curves of SAC177, SAC177-0.2Te and SAC177-0.5Co alloys at 25 °C at different strain rates and prior strain rate dependence of imposed strain

Table 1 Material parameters for SAC (177), SAC (177)-0.2Te and SAC (177)-0.5Co alloys obtained from stress relaxation(SR) tests at initial stress $\sigma_i = 10$ MPa and constant temperature of 25 °C; prior strain rate $\dot{\epsilon}$, imposed strain ϵ_0 , final applied load σ_f (MPa), amount of relaxed stress ($\Delta\sigma$), relaxed stress percentage $\Delta\sigma\%$, stress relaxation rate σ' and stress exponent n

Alloy	$\dot{\epsilon}$	ϵ_0	σ_f	$\Delta\sigma$	$\Delta\sigma\%$	σ'	n
SAC 177	6.6×10^{-5}	0.0020	2.36	7.64	76.4	0.897	8.2
	2.5×10^{-4}	0.0023	3.50	6.5	65	0.763	7.4
	5.8×10^{-4}	0.0024	3.87	6.13	61.3	0.719	6.2
	1.4×10^{-3}	0.0038	4.69	5.31	53.1	0.623	6
	3.5×10^{-3}	0.0045	5.63	4.37	43.7	0.513	5.8
SAC 177-0.2Te	6.6×10^{-5}	0.0021	2.87	7.13	71.3	0.837	9.1
	2.5×10^{-4}	0.0025	3.41	6.59	65.9	0.773	8
	5.8×10^{-4}	0.0030	4.09	5.91	59.1	0.693	7.4
	1.4×10^{-3}	0.0052	5.49	4.51	45.1	0.529	7.1
	3.5×10^{-3}	0.0086	5.98	4.02	40.2	0.472	6.8
SAC 177-0.5Co	6.6×10^{-5}	0.0043	3.44	6.56	65.6	0.770	9.8
	2.5×10^{-4}	0.0046	3.81	6.19	61.9	0.727	9.1
	5.8×10^{-4}	0.0060	5.12	4.88	48.8	0.573	8.9
	1.4×10^{-3}	0.0066	5.87	4.13	41.3	0.485	8.4
	3.5×10^{-3}	0.0130	6.24	3.76	37.6	0.441	7.6

solders (Table 1). This was an unexpected result that elucidates the short-term SR history dependence established by these solder alloys. This phenomenon is in good agreement with previous observation on SR test for copper wires [15, 16]. Nonetheless, this occurrence contrasts to that reported by Woodmansee and Neu [12], where the cyclic prior deformation rates result in larger amount of stress relaxation and smaller relaxed stress for Sn–2.5Ag–0.8Cu–0.5Sb, Sn–4Ag and Sn–40Pb samples. They attributed this behavior to the decrease in the ratio of back stress/total stress. Majors and Krempl [17], Yaguchi and Takahashi [18] also proposed that the cyclic response dependent phenomena is unique and emphasize the non-linear relation between strain rate and relaxation stress. That means, increasing the cyclic strain rate causes less increase in the relaxation stress.

3.4 Stress exponent

In the present study, different SR behaviors of SAC177 based-solders have been conducted with initial stress σ_0 of 10 MPa in the elastic region and the corresponding deformation mechanisms will be assessed in this section. During the SR process, the total imposed strain ϵ_0 of specimen is kept constant. At any time t during SR test, SR occurs because of a part of ϵ_0 is converted into plastic strain ϵ_p . Hence, the total imposed strain ϵ_0 can be directly expressed as:

$$\epsilon_0 = \epsilon_e + \epsilon_p = \text{Const.} \quad (1)$$

Since ϵ_0 is held constant, then the rate of change of $\epsilon_0 = 0$. Equation (1) can be by rewritten as:

$$d\epsilon_p/dt = -d\epsilon_e/dt = -d(\sigma/E)/dt \quad (2)$$

where ϵ_e is the elastic strain, σ is the current stress at any time t and $E = \sigma/\epsilon_e$ is the elastic modulus. The elastic modulus E is determined as 28.6, 29.0 and 29.5 GPa for SAC177, SAC177-0.2Te and SAC177-0.5Co solders, respectively.

Therefore, $d\epsilon_p/dt$ is considered as the creep strain rate from SR test. The relationship between strain rate $\dot{\epsilon}$ and stress σ for the three solders at 25 °C can be attained from Eq. 2 and plotted in Fig. 7a. Besides, the effect of temperature on $\dot{\epsilon}$ versus σ curves for SAC177 solder is illustrated in Fig. 7b. It is interesting to note that the three curves are coincident in first stage of relaxation below ~5 MPa, although they are separated in second the stage above 5 MPa. This result indicates that SR tests are not respond to applied stresses lower than the 5 MPa level, even if the SR tests were conducted at higher temperatures. Additionally, Fig. 7a shows that the relaxation strain rate of SAC177 is greater than that of SAC177-0.2Te and SAC177-0.5Co in the secondary stage of SR. That means, Te and Co microalloying enhanced the creep resistance of SAC177 solder. Also, in the 2nd SR stage, a certain stress and temperature could yield different SR rates for three samples. This suggests that SR rate is affected by the transient stress in the 1st stage and processing temperature. In this case, dislocation motion could grow quickly as the critical stress of 5 MPa can be merely overcome. Based on the power-law equation, the global strain rate $\dot{\epsilon}_p$ is correlated with relaxing stress σ by the following relation [19]:

$$\dot{\epsilon}_p = A\sigma^n \quad (3)$$

For assessing the stress exponent n , the natural logarithm of Eq. 3 is rearranged as:

$$\ln \dot{\epsilon}_p = \ln A + n \ln \sigma \quad (4)$$

Figure 8 shows the steady strain rate versus stress curves of entire alloys in log–log from SR tests. The n values were determined from the slope of $\ln \dot{\epsilon}_p - \ln \sigma$. It can be seen that n values are increased respectively, from 5.8 to 6.8 and 7.6 with Te and Co microalloying at constant $\dot{\epsilon} = 3.5 \times 10^{-3} \text{ s}^{-1}$ and $T = 25 \text{ }^\circ\text{C}$. However, the variations of n values with increasing strain rate are listed in Table 1, while the

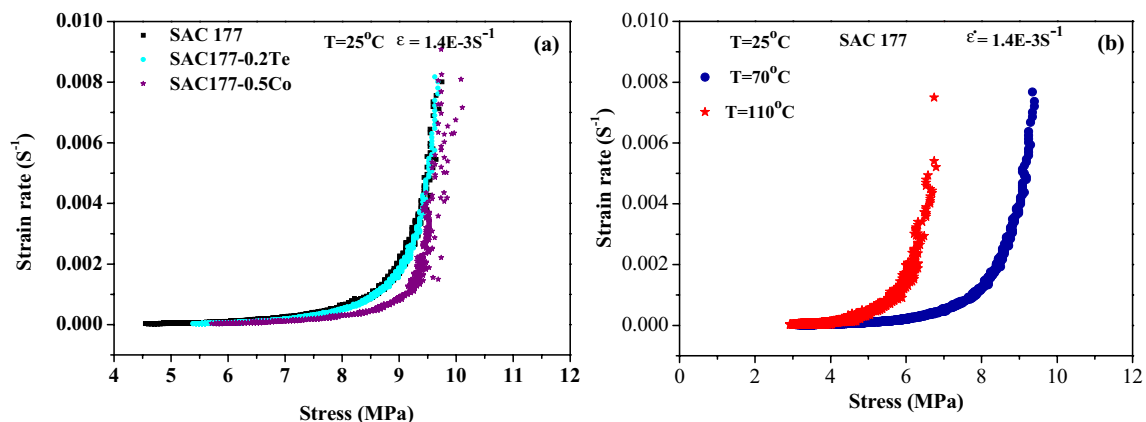


Fig. 7 Global stress dependence of strain rate for of SAC177, SAC177-0.2Te and SAC177-0.5Co alloys at 25 °C

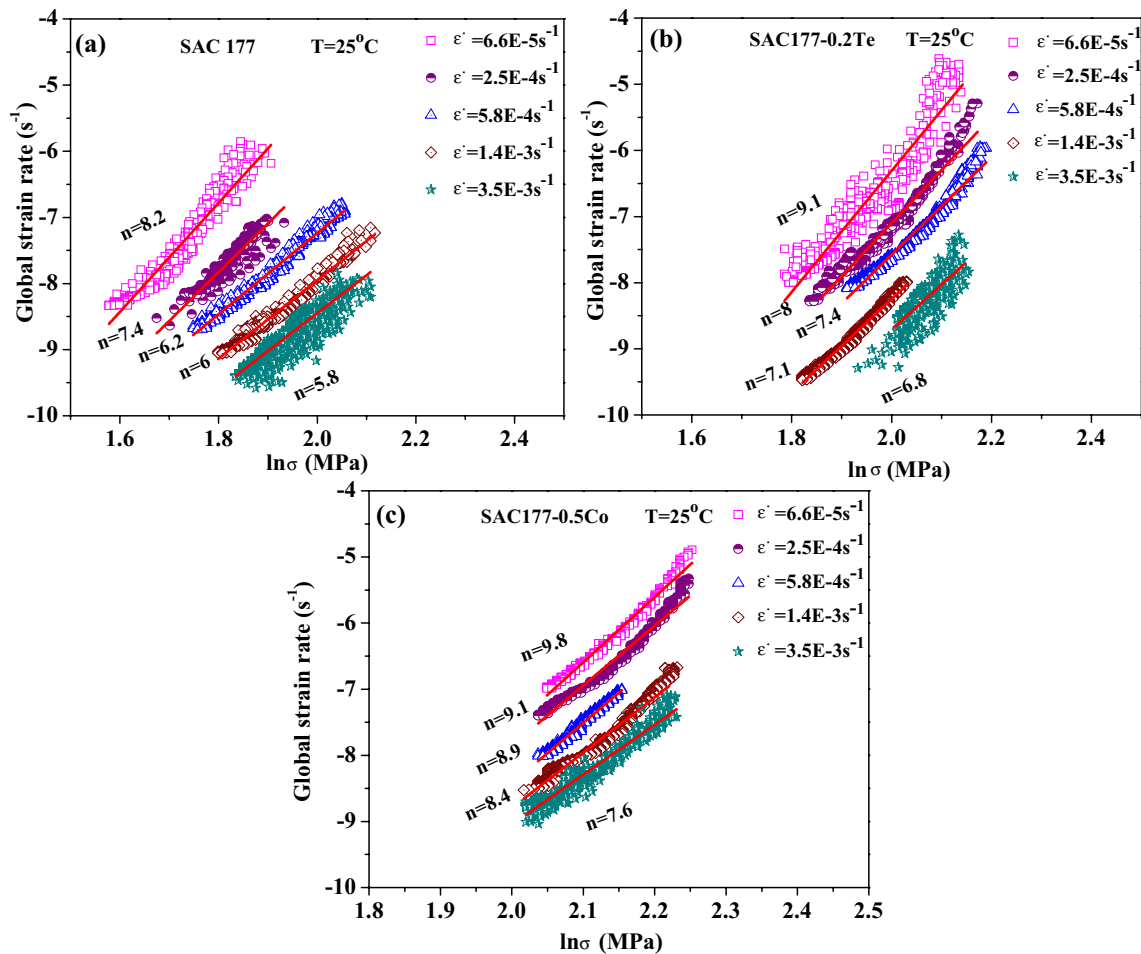


Fig. 8 Global strain rate dependence of stress for SAC177, SAC177-0.2Te and SAC177-0.5Co alloys at 25 °C derived from SRT at different prior strain rates

variations of n with temperatures for three alloys are summarized in Table 2. Interestingly, the n -value for power-law creep was found to depend on the imposed strain or strain rate, wherein it can decrease with increasing strain rate and/or deformation temperature, as shown in Fig. 9. Besides, the higher n values were observed with Te and Co microalloying. The slight drop of n value with increasing temperature for Te- and Co-containing solders indicates the higher stability of its microstructure, and could be attributed to the high dissipation ability of heat by the new SnTe and $(\text{Cu}, \text{Co})_6\text{Sn}_5$ IMCs that developed in the alloy matrix and impeding the dislocation motion, which restrains the SR process. However, stress exponent reflects the deformation mechanism in a sense. Generally, the n values which approach 4–7 indicate climbing of dislocations [7–9].

3.5 Activation energy during hot deformation

Generally, the deformation process of alloy materials is controlled by diffusion mechanism [7, 8]. The

Table 2 Activation energy (Q), stress exponent (n) values for SAC(177), SAC(177)-0.2Te and SAC(177)-0.5Co solder alloys at different temperature and constant strain rate $\dot{\epsilon} = 3.5 \times 10^{-3} \text{ s}^{-1}$

Alloys	Temperature (°C)	N	Q_{exp} (kJ/mol)	$Q_{\text{Theoretical}}$ (kJ/mol)
SAC 177	25	5.8	58.15	63.06
	70	4.5		
	90	4.3		
	110	4.2		
SAC 177-0.2Te	25	6.8	71.10	69.77
	70	5.5		
	90	5.3		
	110	5.1		
SAC 177-0.5Co	25	7.6	78.23	75.48
	70	6.7		
	90	6.5		
	110	6.1		

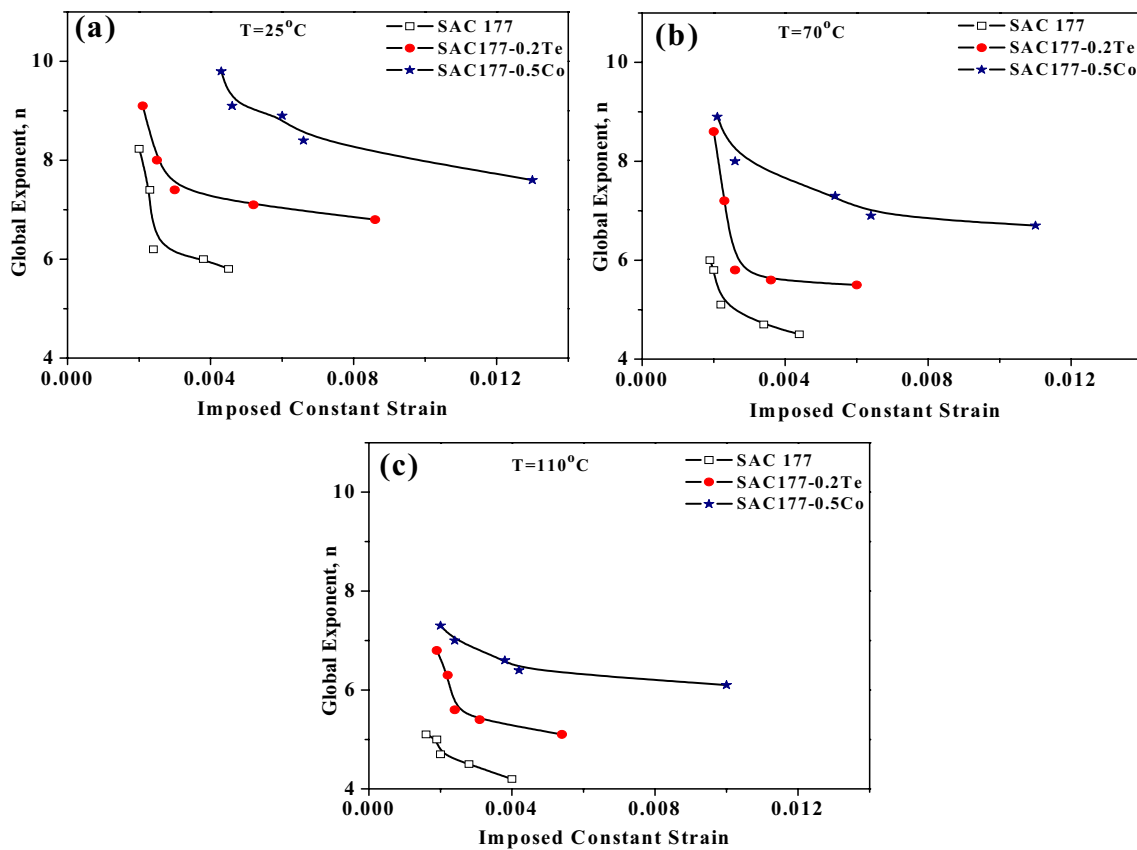


Fig. 9 Imposed strain dependence of stress exponent n derived from SRT at 25, 70 and 110 °C for SAC177, SAC177-0.2Te and SAC177-0.5Co alloys

development of the global strain rate $\dot{\epsilon}_p$ during SR tests as a function of relaxing stress σ and deformation temperature T can be mathematically appointed with the Arrhenius power-law equation [19] as:

$$\dot{\epsilon}_p = A\sigma^n \exp(-Q/RT) \tag{5}$$

where Q is the activation energy, R is the gas constant, A is the creep constant and n is the stress exponent. The Q values can be evaluated from:

$$Q = Rn \left[\frac{d \ln \sigma}{d \left(\frac{1}{T} \right)} \right] \dot{\epsilon}_p \tag{6}$$

The logarithmic relationship between relaxation stress $\ln \sigma$ and $1000/T$ (K^{-1}) at strain rate of $3.5 \times 10^{-3} s^{-1}$ is presented in Fig. 10. By linear fitting, the Q values of 58.15, 71.10 and 78.23 $kJ mol^{-1}$ for SAC177, SAC177-0.2Te and SAC177-0.5Co solder alloys, respectively; can be matched well with the grain boundary diffusion mechanism [7–9, 18]. These Q values indicate that the activation energy of SAC177 based-solders varies with the relaxation

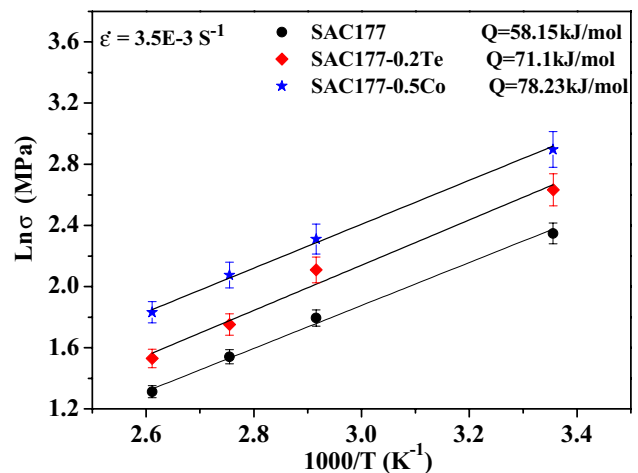


Fig. 10 The activation energy (Q) values of SAC177, SAC177-0.2Te and SAC177-0.5Co alloys at constant strain rate $3.5 \times 10^{-4} s^{-1}$

stress, stress exponent and testing temperature according to Eq. (6).

In an attempt to establish the mechanism of stress relaxation, a quantitative analysis has been carried out on the

experimental results based on single barrier model of logarithmic SR [15]. The SR rate $\dot{\sigma}$ in this model has been represented as a function of activation energy Q , initial stress σ_0 of relaxation and temperature T by the relation:

$$\dot{\sigma} = [kT\sigma_0/(Q - mkT)] \quad (7)$$

where k is Boltzmann constant and the constant $m = 25$. By differentiating Eq. 7 with regard to σ_0 , one can obtain the Q values of three solders, as:

$$(d\dot{\sigma}/d\sigma_0) = [kT/(Q - mkT)] \quad (8)$$

$$Q = kT[m + (d\sigma_0/d\dot{\sigma})] \quad (9)$$

The unit of Q values designed from Eq. (9) is eV. However, Eq. (9) can be reserved. Here, as is striking, we replace the constant m by stress exponent n values and the Boltzmann constant k by gas constant R . Thus one has:

$$Q = RT[n + (d\sigma_0/d\dot{\sigma})] \quad (10)$$

The unit of Q values designed from Eq. (10) is kJ mol^{-1} . The attained Q values of the relaxation process from the empirical formula in Eq. (10) at room temperature are; 63.06, 69.77 and 75.48 kJ mol^{-1} for SAC177, SAC177-0.2Te and SAC177-0.5Co solder alloys, respectively. These Q values are close to that obtained from Eq. (6), as seen in Table 2. The numerical Q value results illustrate that the developed relaxation model can describe the inelastic deformation of SAC177, SAC177-0.2Te and SAC177-0.5Co alloys with good accuracy. Moreover, the Q values are in the order of magnitude of grain boundary diffusion mechanism. They are somewhat small to be associated with the lattice diffusion mechanism (90–120 kJ mol^{-1}) [7, 8, 20]. Interestingly, the calculated Q values from the modified relaxation model are in good agreement with Q values from the present experimental results. Alternatively, Eq. (10) also implies that the modified relaxation model could better confirm the SR rate $\dot{\sigma}$ dependence of kinetic parameters, wherein $\dot{\sigma}$ is decreased with increasing Q values, and hence with Te/Co addition to SAC177 solders (as seen in Fig. 6). This could be ascribed to the amount of unrelaxed dislocation pile-ups that growing at the interface boundaries of SnTe and $(\text{Cu,Co})_6\text{Sn}_5$ IMCs in the path of an elastic relaxation. These accumulated dislocation pile-ups could induce incessant reduction in the movement of further dislocations arriving from inside the crystal lattice. And could result in an associated reduction in the SR level and SR rate of SAC177-0.2Te and SAC177-0.5Co alloys; the greater the interface boundaries of IMCs, the better the hindering effect, and hence the minimum the amounts of SR and SR rate. Similar behavior was observed for Cu–42.2Zn–0.6Pb alloys [16]. The variations in solidification mode and its structural effects, such as the SR level and SR rate, suggest that a single barrier model is not sufficient to explain increasing Q values pertaining to the

relaxation stress, since the n values are changed with varying deformation temperature.

4 Conclusions

- (1) Te and Co microalloying enhanced both the strength and ductility of SAC177 alloy. This is a significant issue, which develops the elastic compliance and impact resistance of solder joints assembled in SAC177 alloys.
- (2) The achieved strength improvement is activated by precipitation hardening effects of SnTe and Co_3Sn IMCs in the respective alloys, while the enriched ductility of Te- and Co-containing alloys can be ascribed to structural refinement caused by the microalloying.
- (3) According to the modified single barrier model of logarithmic stress-relaxation, the amount of SR and SR rate of SAC177 solder were significantly decreased with increasing prior strain rate, Q value and Te/Co addition.
- (4) The structural relaxation of SAC177 solders occurred at high prior deformation history could induce unexpected relaxation resistance that depends on the qualified proportions of Te and Co microalloying, high prior deformation results in both low SR levels and SR rates.
- (5) According to the obtained n and Q values, the dominant deformation mechanism in of SAC177 and Te-containing alloys is dislocation climb with pipe diffusion over the entire temperature range examined. The Q values obtained from the modified relaxation model are consistent with the experimental results.

References

1. F. Wang, H. Chen, Y. Huang, L. Liu, Z. Zhang, *J. Mater. Sci.* **30**, 3222–3243 (2019)
2. A.K. Gain, L. Zhang, *Materialia* **5**, 100234 (2019)
3. S. Cheng, C.-M. Huang, M.I. Pecht, *Microelectron. Reliab.* **75**, 77–95 (2017)
4. J. Wu, S. Xue, J. Wang, M. Wu, *J. Alloys Compd.* **784**, 471–487 (2019)
5. W. Jie, S. Xue, J. Wang, M. Wu, *J. Mater. Sci.* **29**, 7372–7387 (2018)
6. H. Wang, K. Zhang, M. Zhang, *J. Alloys Compd.* **781**, 761–772 (2019)
7. A.A. El-Daly, A.E. Hammad, G.S. Al-Ganainy, M. Ragab, *J. Alloys Compd.* **614**, 20–28 (2014)
8. A.A. El-Daly, A.E. Hammad, G.S. Al-Ganainy, M. Ragab, *Mater. Sci. Eng. A* **608**, 130–138 (2014)
9. A.A. El-Daly, A.M. El-Taher, S. Gouda, *Mater. Des.* **65**, 796–805 (2015)
10. M.B. Zhou, X.F. Zhao, W. Yue, X.P. Zhang, *J. Mater. Sci.* **30**, 4770–4781 (2019)
11. A.A. El-Daly, A.A. Ibrahim, *J. Alloys Compd.* **740**, 801–809 (2018)

12. M.W. Woodmansee, R.W. Neu, *Mater. Sci. Eng. A* **322**, 79–88 (2002)
13. G. Saad, S.A. Fayek, A. Fawzy, H.N. Soliman, *Gh Mater. Sci. Eng. A* **527**, 904–910 (2010)
14. Q.B. Tao, L. Benabou, V.N. Le, H. Hwang, D.B. Luu, *J. Alloys Compd.* **694**, 892–904 (2017)
15. M.Z. Butt, M.S. Khiliji, *J. Alloys Compd.* **479**, 252–256 (2009)
16. S. Guo, Y. He, Z. Li, J. Lei, D. Liu, *Inter. J. Plast.* **112**, 278–296 (2019)
17. P.S. Majors, E. Krempl, *Mater. Sci. Eng. A* **186**, 23–24 (1994)
18. M. Yaguchi, Y. Takahashi, in *Constitutive modeling and damage modeling of inelastic deformation and phase transformation*, ed. by A.S. Khan (Neat Press, Fulton, 1998), pp. 103–106
19. J. Luo, W. Xiong, X. Li, J. Chen, *Mater. Sci. Eng. A* **743**, 755–763 (2019)
20. A.R. Geranmayeh, G. Nayyeri, R. Mahmudi, *Mater. Sci. Eng. A* **547**, 110–119 (2012)

Publisher's Note Springer Nature remains neutral with regard to jurisdictional claims in published maps and institutional affiliations.